2016 IEEE International Conference on Robotics and Automation (ICRA)
Stockholm, Sweden, May 16-21, 2016

Unscented Kalman Filter and 3D Vision to Improve Cable Driven Surgical Robot Joint Angle Estimation

Mohammad Haghighipanah[1], Muneaki Miyasaka[2], Yangming Li[1], and Blake Hannaford[3]

Abstract— **Cable driven manipulators are popular in surgical robots due to compact design, low inertia, and remote actuation. In these manipulators, encoders are usually mounted on the motor, and joint angles are estimated based on transmission kinematics. However, due to non-linear properties of cables such as cable stretch, lower stiffness, and uncertainties in kinematic model parameters, the precision of joint angle estimation is limited with transmission kinematics approach. To improve the positioning of these manipulators, we use a pair of low cost stereo camera as the observation for joint angles and we input these noisy measurements into an Unscented Kalman Filter (UKF) for state estimation. We use the dual UKF to estimate cable parameters and states offline. We evaluated the effectiveness of the proposed method on a Raven-II experimental surgical research platform. Additional encoders at the joint output were employed as a reference system. From the experiments, the UKF improved the accuracy of joint angle estimation by 33-72%. Also, we tested the reliability of state estimation under camera occlusion. We found that when the system dynamics is tuned with offline UKF parameter estimation, the camera occlusion has no effect on the online state estimation.**

Index Terms— **surgical robots, cable driven mechanism, flexible manipulators, Unscented Kalman Filter.**

I. INTRODUCTION

Cable driven manipulators have a long history and they are found in many applications including advanced Robotic Surgical Assistants (RSAs) such as such as da Vinci® [1] and Raven-II ® [2]. Cable driven mechanisms consist of rigid links, cables, capstans, and pulleys. Usually a cable is multiply wrapped in a figure eight shape around input and output capstans to achieve high stiffness [3]. In these manipulators, power is transmitted through cables to move the end-effector to the desired position and actuators can be installed remotely from the driven axes. This kind of power transmission provides several advantages over non-cable driven mechanisms including lower inertia, structural simplicity, compact design, and remote actuation. Remote installation of the actuators realizes lightweight and compact design. Low inertia reduces the energy that is needed to move the link which is desirable in robot applications. Also, in a fully cable driven manipulator, sensitive parts are located away from the end-effector, which is then suitable for harsh environments [4], [5], [6]. In RSAs, due to sterilization, placement of tracking sensors or encoders on the end-effector is difficult [7]. In Raven, all the encoders are mounted on the shaft of the motors away from the joints. The joint angles are estimated from **transmission kinematics**: gear ratios, pulley ratios, cable couplings which define the mapping from motor rotations to joint rotations.

However, the use of cable in robot manipulators introduces new challenges to control of the systems due to elasticity of cables and their nonlinear properties [7]. Moreover, cables transmits power thorough tension and therefore to treat them as a rigid link, the cables must remain under tension [7], [5]. Also, compared to rigid links, the stiffness of cable is lower, which may cause undesirable vibrations [5] and a relative position error between motor and link [7]. If cable elasticity is not modeled in dynamic equations and an appropriate control compensation is not considered, the accuracy of a cable driven robot is limited. In tele-operating RSAs, these inaccuracies are compensated by surgeon's visual feedback and skill. However, for autonomous surgical tasks, appropriate control compensation is required.

Stereo vision is becoming more common in RSAs [8]. In [8], stereo vision and a model predictive controller (MPC) were used to perform a simulated debridement task (an automated surgical sub-task to remove dead tissues). In [9], Gaussian Process Regression (GPR) was used to learn accurate kinematic control by including velocity as a feature and removing corrupted observations from a pre-recorded data set. Four high speed cameras with active LED's were used for motion detection and the authors acknowledged the sensitivity of this method to sensor noise.

To improve the accuracy of cable driven robots, state estimation techniques can be adopted. For non-linear systems, Unscented Kalman Filter (UKF) [10] can be used for state estimation. UKF uses deterministic sampling technique and it is simple to implement [11]. Previously the UKF was used in [12] to estimate states of a one DOF cable driven test panel, and in [13], the UKF was applied on a multi-link simulated robot.

In [14], the work on the UKF was extended by applying it to the first 3 DOF of the Raven to estimate cable coupling parameters offline and estimate joint angles online. The UKF improved the state estimation online even by observing only motor encoders. However, in offline parameter estimation, both motor encoders and joint encoders were used to estimate parameters. Furthermore, the feasibility of estimating the system parameters offline without using ideal high resolution joint encoders were not studied. Moreover, the result shows that for more rigid joints the transmission kinematic errors are dominant and the UKF does not provide improvements.

[1]Mohammad Haghighipanah (mpanah@uw.edu) and and Yangming Li (ttymli81@uw.edu) Department of Electrical Engineering
[2]Muneaki Miyasaka (muneaki@uw.edu) Department of Mechanical Engineering.
[3]Blake Hannaford (blake@u.washington.edu) Departments of Electrical Engineering, Mechanical Engineering, and Surgery
University of Washington, Seattle, WA 98195, USA

Also, the results were based on an ideal sinusoidal trajectory and statistical analysis were not performed.

The overall goal of this work is to improve the accuracy of position control in RSA with practical sensors. Specifically, in this paper we use the joint sensors of [14] only for validation and all the parameter identification is performed with stereo vision. Moreover, we extend the previous work to 1) estimate kinematic model parameters of the rigid joints in addition to the dynamic model parameters to improve joint angle estimation, 2) perform realistic trajectories to test the effectiveness of the method, 3) verify the system performance and the estimator convergence when the camera is occluded. To evaluate the proposed method, we use the first three DOF of the Raven. The experimental setup is shown in Fig. 1.

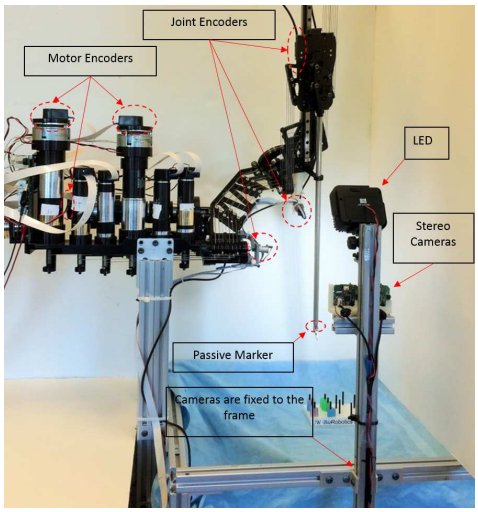

Fig. 1. Raven-II experimental research platform. Joint encoders are mounted on each joint for validation only and their values were not used in the controller or the UKF. Stereo cameras, fixed perpendicular to the robot base, were used for stereo 3D vision.

II. VISION

A. Hardware

We place a passive visual marker on the tip of the robot and use stereo vision to track the tip in real-time. For stereo vision, we constructed a low cost stereo camera using a pair of "Logiteck QuickCam Communicate MP" cameras with baseline of 48.0 mm and resolution of 640x480 pixels at 15 Frame Per Second (FPS). We fixed the cameras perpendicular to the stand of the robot (Fig. 1). To calibrate the cameras' intrinsic parameters, we used a checkerboard and the ROS $camera\_calibration$ package [15]. Once the cameras' intrinsic parameters were known, the translation offset between the origin of the camera frame and the origin of the marker frame (${}^{C}P_{C,M}$) were calculated from the projection of a rectified pixel with disparity to a 3D point.

To register the camera to robot frame, the transformation between camera frame and the robot frame must be found. In Raven, the location of the end-effector is computed in frame zero [16] and since the cameras are fixed perpendicular to the robot's base, the rotation matrix from cameras to the robot frame zero (${}^{C}_{0}R$) is known. However the translation offset needs to be found.

In Raven, encoders are initialized at the hard-stop position (the physical joint limit position of each joint). Thus at the hard-stop position, there is no kinematic error. Furthermore, at this position from kinematics, the translation offset between the origin of frame zero and the origin of the end-effector (marker) ${}^{0}P_{0,M}$ is known. Since in this work, we are only tracking translation, we can assume there is no rotation between frame zero and the origin of the marker. Hence, they are coincident (${}^{0}_{M}R = Identity$). Thus, the homogeneous transformation from the camera to the marker ${}^{C}_{M}T$ is known at this point with translation vector ${}^{C}P_{C,M}$ and rotation matrix ${}^{C}_{M}R = {}^{C}_{0}R$. Also, the homogeneous transformation between frame zero to marker (${}^{0}_{M}T$) is known with translation vector ${}^{0}P_{0,M}$ and rotation matrix ${}^{0}_{M}R$. Hence, the transformation from camera frame to frame zero can be calculated by:

$$ {}^{C}_{0}T = {}^{C}_{M}T({}^{0}_{M}T)^{-1} \tag{1} $$

This method works under the assumption that the camera is mounted perpendicular to the robot and the rotation matrix (${}^{C}_{0}R$) is known. If these constraints are not set, the full transformation can be obtained by placing multiple markers on the tip with known initial kinematics offset at the hard-stop position. However, this still assumes that the camera is fixed to the base.

B. Methods

To track the end-effector position, we placed a passive color-marker on the tip of the robot and used stereo vision hardware described in Section II-A for color-marker detection.

1) Marker Detection: To localize and segment the color-marker, we assumed that no other object with the same color is present in the cameras' field of view. With this constraint, we segment the image with the following procedures. First, we threshold the image based on Hue, Saturation, and Value (HSV). Then, to remove the noise, we smooth the image by applying a median blur filter with kernel size of 5x5 aperture. We also applied the morphological erosion and dilation operations to remove any potential small blobs. Finally, by applying a contour (chain of vectors around the detected marker) and computing its centroid, we found the pixel location of the origin of the marker for each camera. We use the OpenCV library functions [17] to perform these tasks. To calculate the position of the tip in 3D space, we use ROS $image\_geometry$ package [15] to find the disparity map between left and right cameras. These procedures are illustrated in Fig. 2.

Performing these tasks for 640x480 pixels is computationally expensive. Also, because the detection is based on HSV, it requires ideal lighting conditions across the workspace. Slight variation in lighting condition may cause no detection at all or multiple false detection. To improve the detection computation performance and reliability we defined a Region of Interest (ROI) based the on current position of the robot.

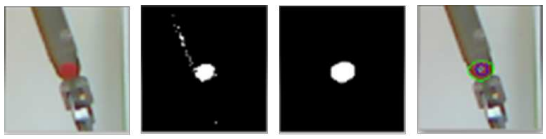

Fig. 2. Marker detection on square ROI. (a) Original 100x100 ROI image taken from right camera around the tip of the Raven. (b) Thresholded image, (c) Processed image after median filter and morphological operations (d) Fitted circle around the detected segment shown in green.

2) Region of Interest (ROI): The kinematics of a cable driven robot may present substantial uncertainties due to lower transmission stiffness. However, the kinematics does provide approximate location of the end-effector from which a ROI can be defined around the tip of the robot. Once a ROI has been implemented, the procedures in Section II-B.1 can be used to detect and localize the marker. By defining a ROI, the detection computation can significantly be improved. The major advantage of this technique is that the search window of the image is much smaller; therefore, the lighting condition does not need to be uniform across the entire workspace. Thus, the upper and lower bound of the HSV can be more relaxed. Therefore, slight variations in lighting conditions will not result in multiple false blob detection. Moreover, since with this technique the detection computation is about 31x faster for 100x100 ROI, a pair of high speed cameras' that supports hardware ROI can be used in real-time for high speed robots.

From Raven forward kinematics, we calculate the approximate position of the end-effector and transform this position into the camera frame (${}^{C}P = {}^{C}_{0}T\,{}^{0}P$). Then, from the cameras' intrinsic parameters, we project ${}^{C}P$ to pixel space of left and right cameras. The ROI is a square of 100x100 pixels around this position for both left and right image. Once the left and right image is updated with ROI, we use the process outlined in Section II-B.1 to detect the Raven tip in camera frame and transformed it to robots' frame by ${}^{0}P = {}^{0}_{C}T\,{}^{C}P$. Then, inverse kinematics were used to calculate joint angles. Throughout this paper, we denote joint angles based on vision as $\hat{q}_C$.

III. SYSTEM DYNAMICS

The dynamic equations of a general cable driven robot in particular the Raven were modeled and described in details in our previous paper [14]. In summary, in a cable driven mechanisms the motors are mounted remotely and the power is transmitted through cables to the joints. Thus, the dynamics of each motor and the transmission can be modeled as:

$$\ddot{q_m} = (1/I_m)(\tau - \tau_m - \tau_{rn}) \tag{2}$$

$$\tau_m = \tau_{cm}\text{sign}(\dot{q_m}) + \tau_{vm}\dot{q_m} \tag{3}$$

$$\tau_{rn} = r_{mc}\gamma/N \tag{4}$$

$$\gamma = k_e(e^{q_{mc}r_{mc}-q_l r_l} - e^{q_l r_l - q_{mc}r_{mc}}) + 2b_e(\dot{q_{mc}}r_{mc} - \dot{q_l}r_l) \tag{5}$$

$$\Gamma = r_l\gamma \tag{6}$$

Where $q_m, \dot{q}_m, \ddot{q}_m$ are motor position, velocity and acceleration, respectively; k_e, b_e are cable stiffness and damping; τ_{cm}, τ_{vm} are motor coulomb and viscous friction; r_{mc}, r_l are capstan radius of motor and link, respectively; N, I_m are the gear ratio and motor inertia of the motors, respectively; τ, Γ are torques on motor and joint, respectively. Therefore, Γ is the actual torque that is transferred to each link. For a serial link manipulator from [18] the dynamic equations can be represented as:

$$\ddot{q_l} = {I_l}^{-1}\left[\Gamma - F_H\left(q_l, \dot{q_l}\right)\right] \tag{7}$$

$$\begin{aligned} F_H\left(q_l, \dot{q_l}\right) &= F_C\left(q_l, \dot{q_l}\right) + F_G + \text{diag}\left(sign(\dot{q_l})\right)F_{cl} \\ &\quad + \text{diag}\left(\dot{q_l}\right)F_{vl} + J^T F_{en} \end{aligned} \tag{8}$$

Where I_l is Inertia matrix; J is Jacobian; F_C are Coriolis and centrifugal terms; F_G is Gravitational force; $q_l, \dot{q_l}, \ddot{q_l}$ are joint position, velocity and acceleration, respectively; F_{cl}, F_{vl} are coulomb and viscous friction, respectively; F_{en} is external torque.

IV. METHODS

A. State Estimation

Raven has four states for each link. The states are motor angle, motor velocity, joint angle and joint velocity. However, an optical encoder with 4000 counts per revolution is mounted directly on the shaft of each motor. Therefore, the position and velocity of the motor is well known and equations 2-4 need not be solved. Hence, the dynamics can be simplified and the system states can be reduced to two states for each link (joint angle, and joint velocity). With this simplification the state space form of the Raven can be expressed as:

$$\begin{aligned} \dot{\mathbf{x}} &= \mathbf{f}(\mathbf{x}, \mathbf{u}) \\ \mathbf{y} &= \mathbf{H}\mathbf{x} \end{aligned} \tag{9}$$

Where $\mathbf{x}$ and $\mathbf{H}$ are system states and the observation matrix, respectively. The system states and observations for the first three links are defined as:

$$\begin{aligned} &\mathbf{x}_i := \begin{bmatrix} q_{l_i} & \dot{q}_{l_i} \end{bmatrix}, i = 1, .., 3 \\ &\mathbf{x} = \begin{bmatrix} x_1 & x_2 & x_3 \end{bmatrix}^T \\ &\mathbf{h_i} := \begin{bmatrix} 1 & 0 \end{bmatrix}, \mathbf{H} = blkdiag(\begin{bmatrix} \mathbf{h_1}, & \mathbf{h_2}, & \mathbf{h_3} \end{bmatrix}) \end{aligned} \tag{10}$$

Where i is the link number and the measurements $\mathbf{y}$ are the joint angles based on noisy camera data. In this work, we use the square root (srUKF) [19] form of the UKF which has improved numerical properties [20]. To solve the differential equation, we use the fourth order Explicit Runga Kutta method. The initial inertia matrices, center of mass, and mass were obtained from CAD models and the joint friction parameters (F_{cl}, F_{vl}) were obtained from [14].

B. Parameter Estimation

Raven system consists of both kinematic model and dynamic model parameters. We used the dual UKF to estimate these parameters. In the dual UKF two parallel filter runs are made for the states and the parameters. When estimating the states the parameters are assumed to be known, and when estimating the parameters the states are assumed to be known [21]. Equation (10) is used for state space representation of states. From [22], the state space representation for parameters is described by:

$$\mathbf{w}_{k+1} = \mathbf{w}_k + \mathbf{r}_k \quad (11)$$

$$\mathbf{d}_k = \mathbf{G}(\mathbf{x_k}, \mathbf{w_k}) + \mathbf{e}_k \quad (12)$$

Where, $\mathbf{w}_k$ is the unknown parameters with identity state transition matrix. $\mathbf{r}_k$ is the process noise. $\mathbf{G}(\mathbf{x_k}, \mathbf{w_k})$ is a nonlinear mapping that is parameterized by the vector $\mathbf{w}$. $\mathbf{d}_k$ is the desired output from nonlinear observation on $\mathbf{w}_k$ and $\mathbf{e}_k$ is the error of the system [23].

1) Kinematic Model Parameters: Many cable driven mechanisms, have gear ratios, cable pulley ratios, and mechanism kinematics. It is very important to know the exact value of each of these parameters for accurate transmission kinematics calculations. Slight variation in any of these parameters can substantially increase the error in calculating the end-effector position from motor angles alone. In Raven, the transmission of joint 1 is very stiff. Thus, transmission kinematic error is dominant vs. error due to cable compliance. This, was observed in [14], where the UKF did not provide any improvements for estimating the joint angles of rigid transmissions.

From kinematics of Raven, the motor angle of link 1 is related to joint 1 angle by: $q_m = N(r_{l1}/r_{m1})q_1$. Where, $N = 12.25$ (gear ratio), $r_{l1} = 63.095mm$ is the design radius of the partial pulley of link 1, and $r_{m1} = 5.675mm$ is the design radius of the motor capstan. However, as it can be seen from Fig. 3 (b) there is a gap between the pulley radius which introduces uncertainty in the pulley ratio. This causes significant error in joint angle estimation. In Raven we verified experimentally that the effective ratio of transmission was different from the actual one on the robot as shown in Fig. 3 (a). To conduct this experiment, we changed the value of r_{l1} from its design value from -10% to +10% and measured the true joint angles directly from joint encoders. To compensate for this source of error, we used the dual UKF parameter estimation and stereo vision to estimate the radius of partial pulley of link 1 (r_l).

2) Dynamic Model Parameters: Over time, the cable parameters such as stiffness and damping can change due to creep and stretch [7], [12]. We used the dual UKF parameter estimation and stereo vision offline to compensate for these changes to improve system dynamics.

V. Experiments

In this paper, the main objective is to improve the state estimation of the joint angles by using the UKF and low cost stereo vision. Therefore, to measure the performance of

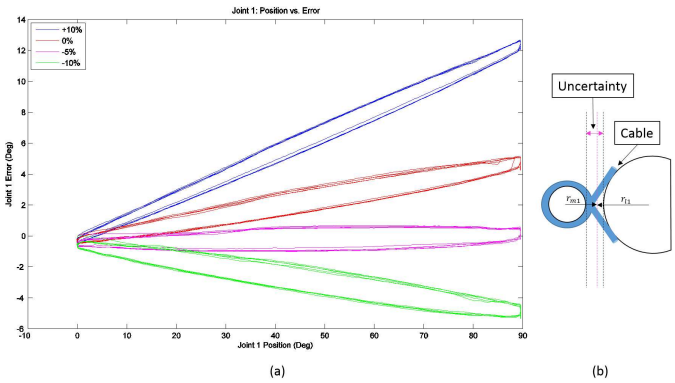

Fig. 3. (a) Joint 1 position error when the value of r_{l1} is changed by +10%, 0%, -5%, -10%. The error decreases to almost zero when the value is changed from its design value by -5%. (b) Schematic drawing of link 1 transmission shows uncertainty in transmission ratios.

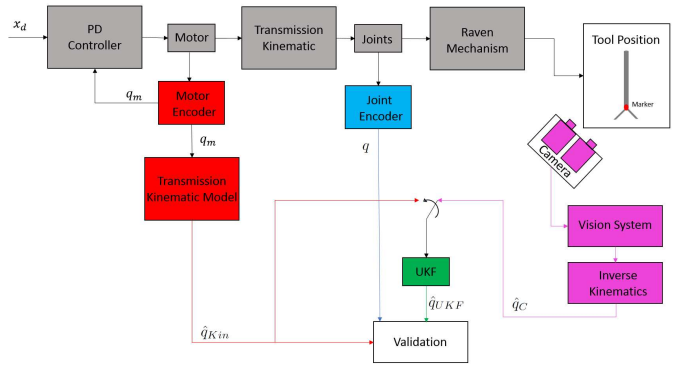

Fig. 4. Block diagram of the controller loop and joint angles. x_d is the desired trajectory. q is the true joint angle measurements from optical encoders mounted directly on the joints. $\hat{q}_{Kin}$, $\hat{q}_C$, and $\hat{q}_{UKF}$ are estimated joint angles from transmission kinematics, camera, and UKF, respectively. The robot controller feedback is based on the motor measurements and not the UKF. When occlusion happens the UKF observation will switch from $\hat{q}_C$ to $\hat{q}_{Kin}$.

the UKF, additional optical encoders (Avago Technologies, model number AEDA-3300, 80000 counts per revolution, for the first two rotary joints and linear optical encoder MicroE Systems, model number Mercury II 1600, resolution 5 μm, for the third prismatic joint) were installed on the joints for comparison. Moreover, since we are only investigating state estimation accuracy of the UKF and not the controller performance, the feedback input of the controller is based on the motor angles and the UKF estimated states were not used in the control. Fig. 4 shows a block diagram representation of the joint angle computations and measurements. q represents the true joint angle. $\hat{q}_{Kin}$ is the estimated joint angle based on transmission kinematics. $\hat{q}_C$ is the estimated joint angle based on camera raw data, and $\hat{q}_{UKF}$ is the estimated joint angle based on UKF method proposed in this paper.

To estimate parameters and states of the Raven, we implemented srUKF in C++ and designed experiments A-D. We used pre-recorded Fundamentals of Laparoscopic (FLS) block transfer task [24] trajectory for experiments B-D, which is one of the five FLS tasks that emulates tissue handling and manipulation [25].

A. Kinematic Model Parameters Estimation

To improve the state estimation, we first estimated the partial pulley radius (r_l) of link 1 offline using the UKF parameter estimation. To estimate r_l of link 1, we ran a sinusoidal trajectory on Raven and we observed the end-effector with the cameras. These observation were used in the UKF dual parameter and state estimation offline.

B. Dynamic Model Parameters Estimation

After finding the updated value of r_l for link 1, we estimated the cable parameters. To estimate cable parameters, a pre-recorded FLS block transfer trajectory was applied on Raven and the cable stiffness (k_e) and cable damping (b_e) parameters of joints 1-3 were estimated with the dual UKF.

C. State Estimation

After finding the kinematic and dynamic model parameters offline, we used the updated parameters to estimate system states online. To test state estimation under realistic conditions, FLS block transfer trajectories in free-space were applied to the control inputs of the Raven PD controller. To conduct statistical analysis, we ran the robot six times with different pre-recorded FLS block transfer trajectories. Each experiment had different duration. The total length of all these six experiments were 900 seconds.

D. Camera Occlusion

The UKF is programmed to detect occlusion. UKF detects occlusion when no marker is detected in either of the cameras or if the marker jumps to a new location. To investigate the system performance and filter convergence under camera occlusion, five experiments with the same FLS block transfer trajectory of 200 seconds were conducted. Each experiment had occlusion for a different percentage of time: 10%, 20% , 40%, 60%, and 80%. To simulate occlusion, we repeatedly blocked the camera data for multiple intervals of 2 seconds at equal time intervals to create the above percentages. During the camera occlusions, the UKF joint observations were changed to $\hat{q}_{Kin}$ with hard switch (Fig. 4), which is calculated from transmission kinematics based on motor encoder measurement.

VI. RESULTS AND DISCUSSION

A. Experiment A

The radius of partial pulley of link 1 (r_l), was estimated based on a 200 seconds sinusoidal trajectory (Fig. 5). The parameter estimation (Fig. 6) converged in about 40 seconds to 59 mm from the initial value of 63.095 mm or a decrease of 6.49%. This is a consistent with experimental results of Fig. 3. From Fig. 3, it can be seen that a decrease of about 5% is required in the value of the pulley ratios to minimize the kinematic error.

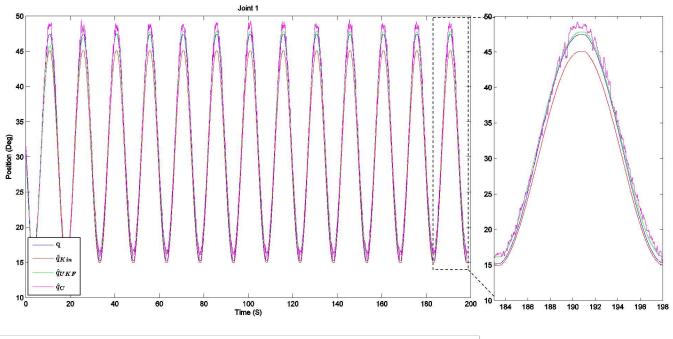

Fig. 5. Plot showing the true position (q), transmission kinematic estimate ($\hat{q}_{Kin}$), UKF estimate ($\hat{q}_{UKF}$), and camera estimate ($\hat{q}_C$). This sinusoidal trajectory was applied on Raven to estimate r_l.

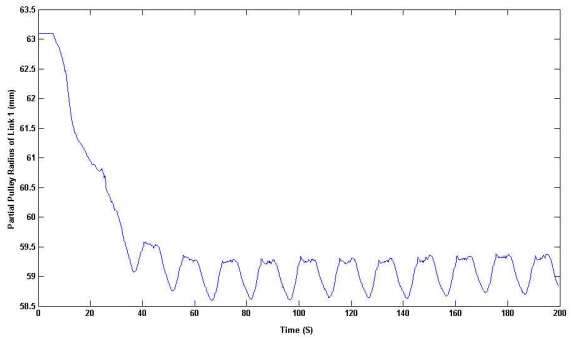

Fig. 6. Estimated r_l parameter for link 1.

B. Experiment B

The dynamic model parameters of the cables, i.e. stiffness and damping, were estimated based on 200 seconds of a pre-recorded FLS trajectory. The results are shown in Fig. 7. The damping values of link 1 and 2 converged in about 100 seconds and the stiffness values of link 1 and 2 converged in about 150 seconds. The stiffness value for link 3 stayed at about the same value and the damping value converged at about 80 seconds.

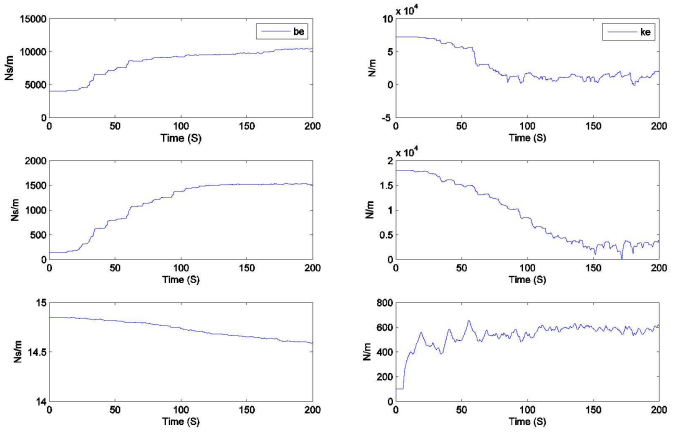

Fig. 7. Estimated cable parameters (stiffness and damping) for link 1-3 from top row to bottom row, respectively.

C. Experiment C

The updated parameters were used for state estimation. Six different FLS block transfer trajectories were performed by the robot. The first FLS trajectory is shown in Fig. 8. The figure illustrates the estimated joint angles with the UKF and direct transmission kinematic for joints 1-3. The joint angles based on camera data and the reference true value from attached ideal joint encoders were also plotted. The corresponding error histogram is shown in Fig. 9. The error using the UKF joint angle estimation for all three joints is less than the error using the direct transmission kinematics method. The results for links 2 and 3 are comparable with [14] where ideal joint encoders were used to tune system parameters. Moreover, the result for the rigid link is substantially improved due to kinematic model parameter estimation.

The results for the remaining five experiments were similar and in all the cases the UKF outperforms transmission kinematics. To perform statistical analysis and summarize the results of all these six experiments the box plot of all these experiments are shown in Fig. 10-12 for joints 1-3, respectively. Furthermore, the joint angle RMS errors using UKF ($e_{\hat{q}_{UKF}}$) and the joint angles RMS errors using transmission kinematics ($e_{\hat{q}_{Kin}}$) for joints 1-3 of trials 1-6 are shown in Table I for comparison. From the table $e_{\hat{q}_{UKF}}$ is less than $e_{\hat{q}_{Kin}}$ for all three joints in all the trials. We took the average of all the trials and use $(100 \times (e_{\hat{q}_{Kin}} - e_{\hat{q}_{UKF}})/e_{\hat{q}_{Kin}})$ to find the percentage improvement that the UKF provides over direct transmission kinematic method for joint angle state estimation. The mean and percent improvements are shown in Table II. When the average was weighted by experiment duration, the results were the same. Also, to verify if there are statistical difference between the $e_{\hat{q}_{Kin}}$ and $e_{\hat{q}_{UKF}}$ we applied Student's t-test. The P values for the t-test are shown in table II. From the t-test it can be concluded that there are significant difference between two groups.

TABLE II

AVERAGE POSITION ERRORS AND PERCENT IMPROVEMENT OF TRIALS 1-6 FOR JOINT 1-3.

Joint (Unit)	$e_{\hat{q}_{UKF}}$	$e_{\hat{q}_{Kin}}$	% Improvement	P value
1 (Deg)	0.7419	1.3051	43.14	0.0025
2 (Deg)	1.6411	2.4652	33.42	0.0015
3 (cm)	0.0790	0.2828	72.05	2.59e-9

D. Occlusion

The results for occlusion experiments are shown in Fig. 13 (a-c) for links 1-3, respectively. We expected that as the occlusion percentage increases, the joint angle estimation error would also increase. However, only slight degradation in quality of state estimation was observed for joint 2 and 3. On the contrary the estimation for joint 1, improved slightly as the occlusion percentage increased. We believe this is because the camera is perpendicular to link 1. Thus, joint 1 is based on the cameras depth measurement (the cameras depth measurements are much more noisier than x and y measurements). Overall, only slight degradation

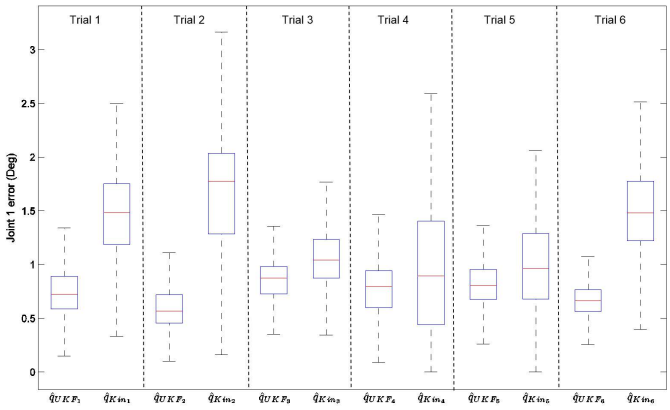

Fig. 10. Boxplot showing the results for Experiment C, for trials 1-6 for joint 1. For each trial, boxplot of UKF estimate and direct transmission estimate is shown for camparison.

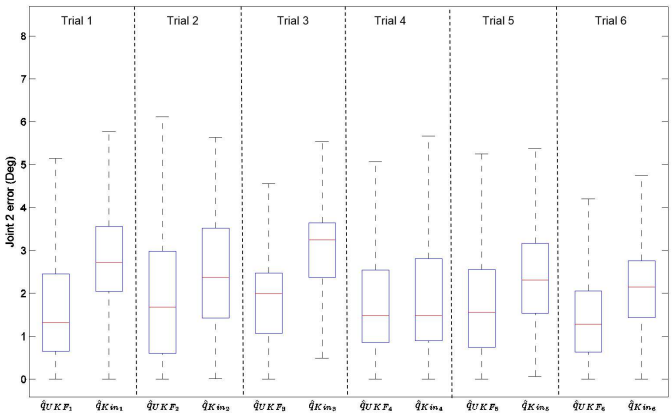

Fig. 11. Boxplot showing the results for Experiment C, for trials 1-6 for joint 2. For each trial, boxplot of UKF estimate and direct transmission estimate is shown for camparison.

and improvement was observed for joint 1-3 as the percent occlusion increased; and therefore, from this experiment, it can be concluded that the UKF estimation is consistent even when occlusion is likely to occur in an application. This suggests that once the system parameters have been identified and fine tuned offline with the UKF and the camera, the UKF will have sufficient information from motor encoders to consistently estimate the states.

VII. CONCLUSION AND FUTURE WORK

In this work, we used motor encoders and low cost cameras to estimate joint transmission parameters of rigid link, cable parameters for all the links, and joint states of a serial cable driven robots on the Raven experimental surgical robot platform utilizing the Unscented Kalman Filter. With this method, we were able to fine tune the system dynamics by estimating parameters offline. Once the dynamics were tuned with UKF parameter estimation, the UKF was able to improve the joint angle estimation. The occlusion experiment suggests that this method is reliable and robust even when the camera is occluded during state estimation. From the experiments, once the system parameters are tuned with stereo vision and the UKF offline, the camera measurements did not

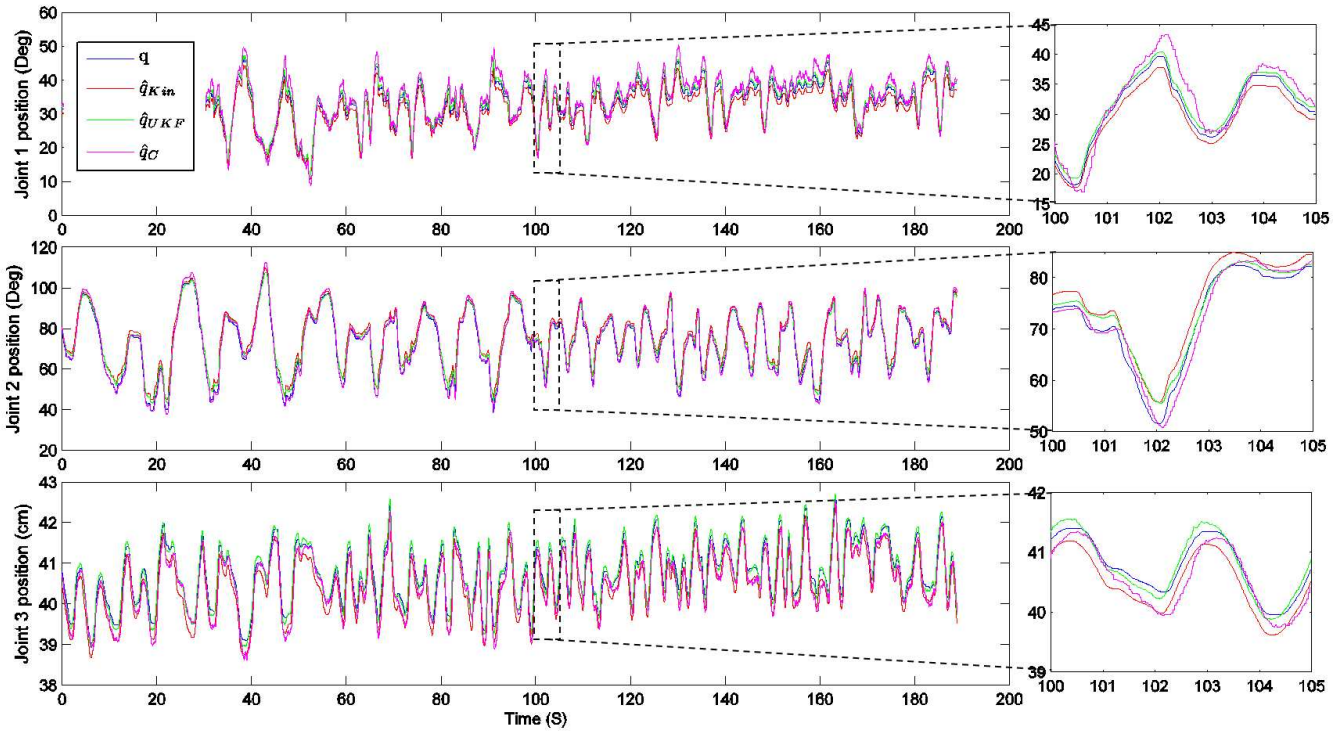

Fig. 8. Actual, transmission kinematics, camera, and UKF estimation of trial 1. Rows 1-3 shows joints 1-3 trajectory, respectively.

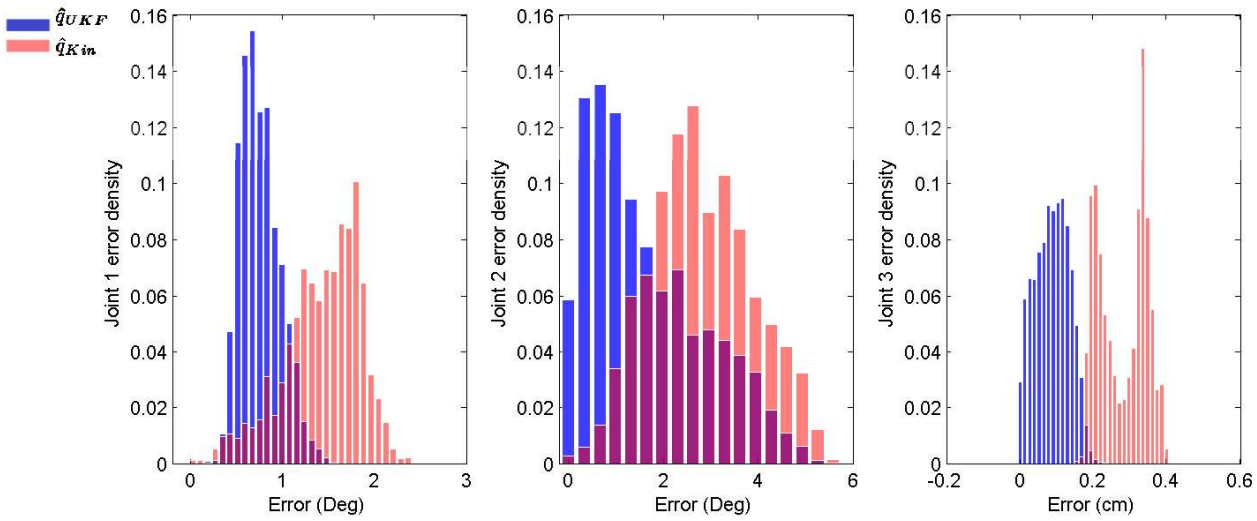

Fig. 9. Error histogram of trial 1 trajectory for joints 1-3 from left to right, respectively.

TABLE I

RMS POSITION ESTIMATION ERRORS OF JOINTS 1-3 FOR EXPERIMENT C TRIALS 1-6.

Joint (Unit)	Trial 1 (188 sec)		Trial 2 (80 sec)		Trial 3 (150 sec)		Trial 4 (82 sec)		Trial 5 (110 sec)		Trial 6 (290 sec)	
	$e_{\hat{q}_{UKF}}$	$e_{\hat{q}_{Kin}}$	$e_{\hat{q}_{UKF}}$	$e_{\hat{q}_{Kin}}$	$e_{\hat{q}_{UKF}}$	$e_{\hat{q}_{Kin}}$	$e_{\hat{q}_{UKF}}$	$e_{\hat{q}_{Kin}}$	$e_{\hat{q}_{UKF}}$	$e_{\hat{q}_{Kin}}$	$e_{\hat{q}_{UKF}}$	$e_{\hat{q}_{Kin}}$
1 (deg)	0.7525	1.4294	0.5958	1.6644	0.8414	1.0847	0.7881	0.9313	0.8167	0.9827	0.6825	1.4675
2 (deg)	1.6373	2.8012	1.8665	2.5525	1.7965	2.9971	1.7541	1.9428	1.7644	2.3691	1.4220	2.1314
3 (cm)	0.0869	0.2792	0.0989	0.3036	0.0606	0.3227	0.0852	0.2647	0.0852	0.2730	0.0763	0.2675

provide much improvement online during state estimation. Hence, only motor measurements and UKF will be sufficient. This is beneficial because in practice the camera will get occluded during surgery. However, running both the camera and motor encoder at the same time improves safety due to redundancy that is provided to estimate joint angles.

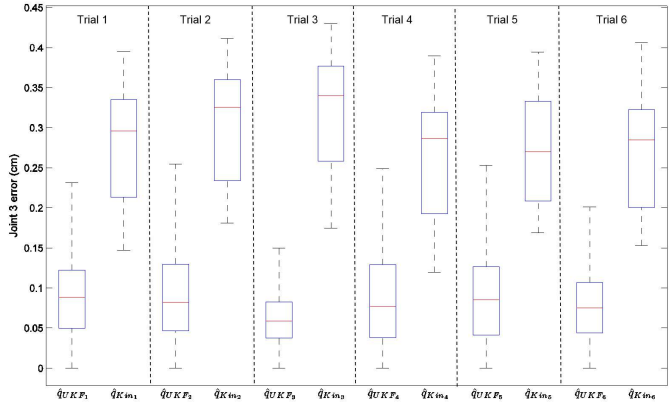

Fig. 12. Boxplot showing the results for Experiment C, for trials 1-6 for joint 3. For each trial, boxplot of UKF estimate and direct transmission estimate is shown for camparison.

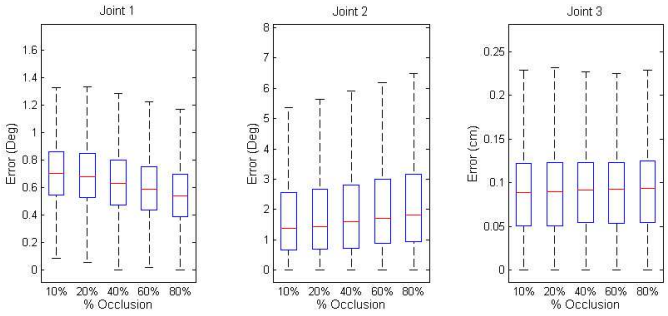

Fig. 13. Boxplot showing the results for Experiment D, for joints 1-3 from left to right, respectively. Each plot shows a boxplot for 10%, 20%, 40%, 60%, and 80% occlusion.

In surgery, in addition to accuracy, redundancy is also important. In case of sensor failures, it is essential to have backup sensors or methods. The future work will include investigating whether the UKF can estimate joint angles using only camera measurements in case of motor encoder failure. Also, we will study for how long and what frequency and speed range the filter can maintain convergence under camera occlusion when a motor encoder fails. Furthermore, we will use the results of ongoing research on improving cable driven mechanism dynamics in [26], which may improve the UKF performance when motor encoder fails.

ACKNOWLEDGMENT

We would like to thank the Korean Institute of Science and Technology (KIST, Dr. Hujoon project), and the National Science Foundation (grant number 1227406) under a subcontract from Stanford University. Also, the authors would like to thank Biorobotics lab, University of Washington and the reviewers.

REFERENCES

[1] G. Guthart and J. K. Salisbury Jr, "The intuitivetm telesurgery system: Overview and application." in *ICRA*, 2000, pp. 618–621.

[2] B. Hannaford et al., "Raven-ii: an open platform for surgical robotics research," *Biomedical Engineering, IEEE Transactions on*, vol. 60, no. 4, pp. 954–959, 2013.

[3] J. Werkmeister and A. Slocum, "Theoretical and experimental determination of capstan drive stiffness," *precision Engineering*, vol. 31, no. 1, pp. 55–67, 2007.

[4] H.-C. Y. J.-J. Lee and M.-S. Chen, "Control for tendon-driven manipulators with flexible tendons using artificial potential field approach," in *12th IFToMM World Congress, Besançon, France*. Citeseer, 2007.

[5] O. Baser and E. I. Konukseven, "Theoretical and experimental determination of capstan drive slip error," *Mechanism and Machine Theory*, vol. 45, no. 6, pp. 815–827, 2010.

[6] S. Behzadipour and A. Khajepour, *Cable-based robot manipulators with translational degrees of freedom*. INTECH Open Access Publisher, 2006.

[7] S. N. Kosari, S. Ramadurai, H. J. Chizeck, and B. Hannaford, "Control and tension estimation of a cable driven mechanism under different tensions," in *International Design Engineering Technical Conferences and Computers and Information in Engineering Conference*. ASME, 2013.

[8] B. Kehoe, G. Kahn, J. Mahler, J.-H. Kim, A. Lee, K. Nakagawa, S. Patil, W. D. Boyd, P. Abbeel, and K. Goldberg, "Autonomous multilateral debridement with the raven surgical robot," in *Robotics and Automation (ICRA), 2014 IEEE International Conference on*. IEEE, 2014, pp. 1432–1439.

[9] J. Mahler, S. Krishnan, M. Laskey, S. Sen, A. Murali, B. Kehoe, S. Patil, J. Wang, M. Franklin, P. Abbeel, *et al.*, "Learning accurate kinematic control of cable-driven surgical robots using data cleaning and gaussian process regression," in *Automation Science and Engineering (CASE), 2014 IEEE International Conference on*. IEEE, 2014, pp. 532–539.

[10] S. J. Julier and J. K. Uhlmann, "A new extension of the kalman filter to nonlinear systems," in *Int. symp. aerospace/defense sensing, simul. and controls*, vol. 3, no. 26. Orlando, FL, 1997, pp. 3–2.

[11] S. J. Julier and J. Uhlmann, "A general method for approximating nonlinear transformations of probability distributions," Technical report, Robotics Research Group, Department of Engineering Science, University of Oxford, Tech. Rep., 1996.

[12] E. Naerum, H. H. King, and B. Hannaford, "Robustness of the unscented kalman filter for state and parameter estimation in an elastic transmission." in *Robotics: Science and Systems*. Citeseer, 2009.

[13] S. Ramadurai et al., "Application of unscented kalman filter to a cable driven surgical robot: A simulation study," in *Robotics and Automation (ICRA), International Conference on*. IEEE, 2012, pp. 1495–1500.

[14] M. Haghighipanah, Y. Li, M. Miyasaka, and B. Hannaford, "Improving position precision of a servo-controlled elastic cable driven surgical robot using unscented kalman filter," in *Intelligent Robots and Systems (IROS), 2015 IEEE International Conference on*. IEEE, 2015.

[15] M. Quigley et al., "Ros: an open-source robot operating system," in *ICRA workshop on open source software*, vol. 3, no. 3.2, 2009, p. 5.

[16] B. Hannaford, J. Ma, H. King, and S. Kosari, "Kinematic analysis of the ravenii(tm) research surgical robot platform," Department of Electrical Engineering, University of Washington, Tech. Rep., 2012.

[17] G. Bradski and A. Kaehler, *Learning OpenCV: Computer vision with the OpenCV library*. " O'Reilly Media, Inc.", 2008.

[18] W. Khalil and E. Dombre, *Modeling, identification and control of robots*. Butterworth-Heinemann, 2004.

[19] R. Van Der Merwe and E. A. Wan, "The square-root unscented kalman filter for state and parameter-estimation," in *Acoustics, Speech, and Signal Processing (ICASSP'01). International Conference on*, vol. 6. IEEE, 2001, pp. 3461–3464.

[20] A. H. Sayed and T. Kailath, "A state-space approach to adaptive rls filtering," *Signal Processing Magazine, IEEE*, vol. 11, no. 3, pp. 18–60, 1994.

[21] J. Gove and D. Hollinger, "Application of a dual unscented kalman filter for simultaneous state and parameter estimation in problems of surface-atmosphere exchange," *Journal of Geophysical Research: Atmospheres (1984–2012)*, vol. 111, no. D8, 2006.

[22] E. A. Wan and R. Van Der Merwe, "The unscented kalman filter for nonlinear estimation," in *Adaptive Systems for Signal Processing, Communications, and Control Symposium. AS-SPCC*. IEEE, 2000, pp. 153–158.

[23] S. S. Haykin, S. S. Haykin, and S. S. Haykin, *Kalman filtering and neural networks*. Wiley Online Library, 2001.

[24] G. M. Fried, "Fls assessment of competency using simulated laparoscopic tasks," *Journal of Gastrointestinal Surgery*, vol. 12, no. 2, pp. 210–212, 2008.

[25] J. Rosen, B. Hannaford, and R. M. Satava, *Surgical Robotics: Systems Applications and Visions*. Springer Science & Business Media, 2011.

[26] M. Miyasaka, J. Matheson, A. Lewis, and B. Hannaford, "Measurement of the cable-pulley coulomb and viscous friction for a cable-driven surgical robotic system," in *Intelligent Robots and Systems (IROS), 2015 IEEE International Conference on*. IEEE, 2015 in Press.